Title

A Novel Pan-Negative-Gating Modulator of KCa2/3 Channels, Fluoro-Di-Benzoate, RA-2, Inhibits Endothelium-Derived Hyperpolarization–Type Relaxation in Coronary Artery and Produces Bradycardia In Vivo

Journal

Molecular Pharmacology, 87(2)

ISSN

0026-895X

Authors

Oliván-Viguera, Aida
Valero, Marta Sofía
Coleman, Nicole
et al.

Publication Date

2015-02-01

DOI

10.1124/mol.114.095745

Peer reviewed

A novel pan-negative-gating modulator of KCa2/3 channels, the fluoro-di-benzoate, RA-2, inhibits EDH-type relaxation in coronary artery and produces bradycardia *in vivo*.

(RA-2, a negative-gating modulator of KCa2/3)

by

Aida Oliván-Viguera, Marta Sofía Valero, Nicole Coleman, Brandon M. Brown, Celia Laría, Mª Divina Murillo, José A. Gálvez, María D. Díaz-de-Villegas, Heike Wulff, Ramón Badorrey, Ralf Köhler

Aragon Institute of Health Sciences I+CS/IIS, 50009 Zaragoza, Spain (A.O.-V., R.K.);

GIMACES, Facultad de Ciencias de la Salud, Universidad San Jorge, 50830 Villanueva de Gállego, Spain (M.S.V., C.L.);

Department of Pharmacology, School of Medicine, University of California Davis, 95616 Davis, CA, USA; (N.C., B.M.B, H.W.)

Departamento de Farmacología y Fisiología, Facultad de Veterinaria, Universidad de Zaragoza, 50013 Zaragoza, Spain (M.D.M.);

Departamento de Catálisis y Procesos Catalíticos, Instituto de Síntesis Química y Catálisis Homogénea (ISQCH), CSIC - Universidad de Zaragoza, 50009 Zaragoza, Spain (M.D.D.V., J.A.G., and R.B.);

Fundación Agencia Aragonesa para la Investigación y Desarrollo (ARAID) (R.K.).

** R.K., R.B., and H.W. contributed equally as senior authors*

Running title: Pan-negative modulation of KCa2/3 channels

Correspondence should be sent to: Ralf Köhler, Unidad de Investigación Traslacional, Instituto Aragonés de Ciencias de la Salud (I+CS), Hospital Universitario Miguel Servet, Paseo Isabel la Católica, 1-3, 50009-Zaragoza. Email: rkohler.iacs@aragon.es

Key words: Coronary artery; endothelium; endothelium-derived hyperpolarization, KCa3.1; KCa2.3; negative-gating modulator; RA-2; small/intermediate-conductance conductance Ca^{2+}-activated K^+ channel; telemetry.

Manuscript information:

Number of pages, 40; number of figures (multi-paneled), 6; tables, 2; supplemental material: Figures S1-S3, and table S1; number of words in Abstract, 239; number of words in Introduction, 890; number of words in Discussion, 1291; number of references, 61.

Non-standard abbreviations: DMSO, dimethyl sulfoxide; EDH, endothelium-derived hyperpolarization; HEK, human embryonic kidney; HR, heart rate; KCa, Ca^{2+}-activated K^+ channel; KCa1.1, large-conductance Ca^{2+}-activated K^+ channel; KCa2, small-conductance KCa channel; KCa3.1, intermediate-conductance Ca^{2+}-activated K^+ channel; hERG, human Ether-à-go-go Related Gene, Kir, inwardly-rectifying K^+ channel, KV, voltage-gated K^+ channel; MAP, mean arterial blood pressure; PCA, porcine coronary arteries; PCAEC, porcine coronary artery endothelial cell, PBS, phosphate buffered saline; RA-1, benzyl 3-fluoro-4-hydroxybenzoate; RA-2, 1,3-phenylenebis(methylene) bis(3-fluoro-4-hydroxybenzoate; RA-3, 1,2-phenylenebis(methylene) bis(3-fluoro-4-hydroxybenzoate; RA-4, 1,4-phenylenebis(methylene) bis(3-fluoro-4-hydroxybenzoate); RA-5, 1,3-phenylenebis(methylene) bis(4-acetamido-3-fluorobenzoate; RA-6, 5-(hydroxymethyl)-1,3-phenylene)bis(methylene) bis(3-fluoro-4-hydroxybenzoate; SKA-31, naphtho[1,2-*d*]thiazol-2-ylamine.

Abstract: KCa2/3 channels are Ca^{2+}/calmodulin-regulated K^+ channels that produce membrane hyperpolarization and shape neurological, epithelial, cardiovascular, and immunological functions. Moreover, they emerged as therapeutic targets to treat cardiovascular disease, chronic inflammation, and some cancers. Here, we aimed to generate a new pharmacophore for negative-gating modulation of KCa2/3 channels. We synthesized a series of mono- and di-benzoates and identified three di-benzoates (RA-2, RA-3, and RA-4) with inhibitory efficacy as determined by patch-clamp. Among them, RA-2 (1,3-phenylenebis(methylene)bis(3-fluoro-4-hydroxybenzoate) was the most drug-like and inhibited human KCa3.1 with an IC_{50} of 17 nM and all three human KCa2 subtypes with similar potencies. RA-2 at 100 nM right-shifted the KCa3.1 concentration-response curve for Ca^{2+}-activation. The positive-gating modulator SKA-31 reversed channel inhibition at nanomolar RA-2 concentrations. RA-2 had no considerable blocking effects on distantly related KCa1.1, Kv1.2/1.3, Kv7.4, hERG, or K_{IR} channels. In isometric myography on porcine coronary arteries, RA-2 inhibited bradykinin-induced endothelium-derived hyperpolarization (EDH)-type relaxation in U46610-precontracted rings. Blood pressure telemetry in mice showed that intraperitoneal application of RA-2 (≤100 mg/kg) did not increase blood pressure or cause gross behavioral deficits. However, RA-2 decreased heart rate by ≈145 bpm, which was not seen in KCa3.1-/- mice. In conclusion, we identified the KCa2/3-negative-gating modulator, RA-2, as a new pharmacophore with nanomolar potency. RA-2 may be of use to generate structurally new types of negative-gating modulators that could help to define physiological and pathomechanistic roles of KCa2/3 in the vasculature, CNS, and during inflammation *in vivo*.

Introduction

KCa2 (Adelman et al., 2012; Köhler et al., 1996) and KCa3.1 (Ishii et al., 1997) channels belong to the gene family of Ca^{2+}/calmodulin-regulated and voltage-independent potassium channels (Wei et al., 2005). Their activation produces solid membrane hyperpolarization that in turns influences electrical excitability and shapes calcium entry through calcium-permeable channels. KCa2 channels (subtypes 2.1, 2.2, and 2.3) are expressed in excitable tissues such as neurons, skeletal muscle, adrenal gland and the heart, and some non-excitable tissues such as the liver and the vascular endothelium, with varying subtype-specific tissue expression profiles (Wei et al., 2005). In neurons, these channels underlie the apamin-sensitive medium afterhyperpolarization and have been suggested to influence refractory times and firing frequency as well as learning and memory (Adelman et al., 2012). In the cardiovascular system, KCa2 channels have been suggested to contribute to cardiac repolarization (Diness et al., 2010; Li et al., 2009), endothelium-derived hyperpolarization (EDH)-type of arterial dilation in response to increased hemodynamics (Edwards et al., 2010; Milkau et al., 2010; Wulff and Kohler, 2013), and to provide a negative feedback on sympathetic tone (Taylor et al., 2003). With respect to pathophysiological relevant functions in humans, recent evidence suggests a role, particularly of the KCa2.3 subtype, in lone atrial fibrillation (Diness et al., 2010; Ellinor et al., 2010), cancer cell migration and metastasis (Chantome et al., 2013), and overactive bladder (Soder et al., 2013).

KCa3.1 channels display a distinct expression pattern and are mostly expressed in non-excitable tissues such as red and white blood cell lineages, secretory epithelia, and the vascular endothelium (Devor et al., 1996; Köhler et al., 2000; Wei et al., 2005; Wulff and Kohler, 2013). Here, hyperpolarization and K^+-efflux through

Ca^{2+}-activated KCa3.1 channels exert physiological functions such as cell volume regulation (Vandorpe et al., 1998), fluid secretions (Devor et al., 1996), and –together with KCa2.3 channels- the EDH-type of arterial dilation specifically to acetylcholine stimulation (Edwards et al., 2010; Wulff and Kohler, 2013). Initially, KCa3.1 has been believed to be an exclusively non-neuronal channel (Ishii et al., 1997; Wei et al., 2005). However, recent evidence suggests possible expression in cerebellar Purkinje cells of the rat (Engbers et al., 2012) and a role of the channel in behavior as suggested by the locomotor hyperactivity in KCa3.1-/- mice (Lambertsen et al., 2012). Besides physiological functions, KCa3.1 channels have been patho-mechanistically implicated in human disease such as arterial endothelial dysfunction (Feletou et al., 2010), cancer growth, cancer cell migration and metastasis (D'Alessandro et al., 2013) and neo-angiogenesis (Grgic et al., 2005), organ fibrosis (Grgic et al., 2009), atherosclerosis (Toyama et al., 2008), neointima formation (Köhler et al., 2003; Tharp et al., 2008) as well as T cell responses (Wulff et al., 2007), and microglia activity (Kaushal et al., 2007). For extensive reviews on the physiological and pathophysiological roles we wish to refer the interested reader to in depth reviews (Feletou et al., 2010; Wulff and Castle, 2010; Wulff and Kohler, 2013). Considering the patho-mechanistic roles of the channels, blockers of KCa3.1 channels emerged as potential drug candidates for the treatment of sickle-cell disease (Ataga and Stocker, 2009), immunosuppression (Wulff and Castle, 2010), asthma (Van Der Velden et al., 2013), fibrosis (Grgic et al., 2009), atherosclerosis (Toyama et al., 2008), and cancer (D'Alessandro et al., 2013; Ruggieri et al., 2012). Positive gating modulators (activators) of KCa3.1 like SKA-31 (Sankaranarayanan et al., 2009) or SKA-111 (Coleman et al., 2014) may serve to improve endothelium-dependent vasodilation and to lower blood pressure (Damkjaer et al., 2012; Köhler et al., 2010;

Mishra et al., 2013; Radtke et al., 2013; Sankaranarayanan et al., 2009; Wulff and Kohler, 2013). Activators of KCa2 channels could be of use to treat epilepsy and ataxia (Shakkottai et al., 2011) while blockers may improve learning and memory. For review see (Lam et al., 2013).

The existing small molecule blockers of KCa3.1 and KCa2 channels are mainly pore blockers (e.g. for KCa3.1: TRAM-34 (Wulff et al., 2001), NS6180 (Strobaek et al., 2013), ICA-17043 (Ataga and Stocker, 2009) that obstruct ion flow at the inner cavity of the channel or at the outer vestibule (i.e. for KCa2: UCL-1684 (Rosa et al., 1998)). However, a caveat is that they may enter the inner cavities of other channels and thereby exert unspecific blocking effects at high dosage. At 10 μM, a concentration often used in cancer related studies, NS6180 inhibits KCa1.1 (BK), Kv1.3 and Kv11.1 (hERG) by more than 50%, while TRAM-34 blocks Kv1.3, Kv1.4, Kv7.2+Kv7.3 and Nav1.4 (Strobaek et al., 2013). Clotrimazole, a related KCa3.1-blocker and cytochromeP450-enzymes blocking antifungal inhibits TRPM8 channels (Meseguer et al., 2008) with submicromolar potencies, and has been shown to modulate TRPV1 and TRPA1 channels that act as receptors for noxius heat/pain and irritants, respectively, in nociceptive neurons (Meseguer et al., 2008), thus limiting the utility of these small molecule blockers for studying KCa3.1 functions at the organ or systemic levels. Therefore, negative-gating modulators of KCa2/3 channels, which interfere with channel gating, could be advantageous over the present pore blockers. So far, two negative-gating modulators, NS8593 (Jenkins et al., 2011) and (-)-B-TPMF (Hougaard et al., 2012) have been described for KCa2 channels. Recently, our screening of a series of phenols and polyphenols identified the synthetic fluoro-tri-benzoic ester, 13b (Lamoral-Theys et al., 2010) (Figure 1 A), as a negative-gating modulator of KCa2/3 channels (Olivan-Viguera et al., 2013). A disadvantage

of 13b is, however, that its high molecular weight (MW 582) and its LogP value of 6.0 violate the Lipinksi “Rule of Five” and make it unlikely that the compound will have oral bioavailability (Lipinski et al., 2001). Moreover, the structure-activity relationship (SAR) accounting for channel inhibition has not been characterized yet. We therefore decided to synthesize less lipophilic and smaller analogues of 13b, which may elucidate the SAR and could serve as templates for structurally new chemical entities for negative-gating modulation of KCa2/3 channels as well as a starting point for the development of subtype-selective negative-gating modulation. Three compounds (RA-2, RA-3, and RA-4; Figure 1 B) were identified as KCa2/3 pan-inhibitors with negative-gating modulator properties and potencies in the nanomolar range. Functionality of RA-2 was further demonstrated by its ability to inhibit EDH-type relaxation of porcine coronary arteries. Telemetric cardiovascular monitoring revealed that RA-2 was apparently safe and did not increase blood pressure, although it reduced heart rate.

Material and Methods:

Synthesis of mono- and di-benzoates: As shown in figure 1 B, monobenzoate RA-1 was obtained by reaction of benzylbromide with 3-fluoro-4-hydroxybenzoic acid. Dibenzoates RA-2, RA-3 and RA-4 were obtained by reaction of the corresponding bis(bromomethyl)benzene with 3-fluoro-4-hydroxybenzoic acid. The dibenzoate RA-5 was obtained by reaction of 1,3-bis(bromomethyl)benzene with 3-fluoro-4-acetamidobenzoic acid. The dibenzoate RA-6 was obtained by reaction of 1,3-bis(bromomethyl)-5-hydroxymethylbenzene with 3-fluoro-4-hydroxybenzoic acid. 3-Fluoro-4-acetamidobenzoic acid was obtained by acetylation of 4-amino-3-fluorobenzoic acid. 1,3-bis(bromomethyl)-5-hydroxymethylbenzene was prepared following literature procedures (Diez-Barra et al., 2001). All reactions were performed in anhydrous dimethylformamide at 105 °C using sodium bicarbonate or potassium carbonate and yielded the corresponding mono- or di-benzoates in 33-60% yields. LogP values were calculated with the program ChemBioDraw-Ultra-13.0. Benzylbromide, 1,2-, 1,3- and 1,4-bis(bromomethyl)benzene, 4-amino-3-fluorobenzoic acid and 3-fluoro-4-hydroxybenzoic acid were purchased from Sigma-Aldrich, Alfa-Aesar, or Fluorochem.

General procedures and physical data: Whenever possible the reactions were monitored by TLC. TLC was performed on precoated silica gel polyester plates and products were visualized using UV light (254 nm) or ethanolic phosphomolybdic acid solution followed by heating. Column chromatography was performed using silica gel (Kieselgel 60, 230–400 mesh). Melting points were determined in open capillaries using a Gallenkamp capillary melting point apparatus and are not corrected. FTIR

spectra were recorded as KBr pellets using a Thermo Nicolet Avatar 360 FT-IR spectrometer, ν_{max} values expressed in cm^{-1} are given for the main absorption bands. ^{1}H NMR and ^{13}C NMR spectra were acquired on a Bruker AV-400 spectrometer operating at 400 MHz for ^{1}H NMR, 100 MHz for ^{13}C NMR and 376 MHz for ^{19}F RMN at room temperature using a 5 mm probe. The chemical shifts (δ) are reported in parts per million and were referenced to the residual solvent peak. Coupling constants (*J*) are quoted in Hertzs. The following abbreviations are used: s, singlet; d, doublet; m, multiplet; bs, broad singlet; dd, doublet of doublets; ddd, doublet of doublets of doublets. High-resolution mass spectra were recorded using a Bruker Daltonics MicroToF-Q instrument from methanolic solutions unless otherwise indicated using the positive electrospray ionization mode (ESI+).

Synthesis of 4-acetamido-3-fluorobenzoic acid: A mixture of 4-amino-3-fluorobenzoic acid (233 mg, 1.5 mmol) and acetic anhydride (459 mg, 425 µl, 4.5 mmol) in anhydrous pyridine (7 ml) was heated at 60 ºC overnight. Then the mixture was concentrated in vacuo, over the residue water (6 ml) was added and then the aqueous solution was acidified with HCl 2N until pH = 1. The product precipitated and was collected by filtration and dried providing 281 mg (95%) of compound 4-acetamido-3-fluorobenzoic acid as a slightly brownish solid. ^{1}H NMR (CD_3OD, 400MHz) δ 2.20 (s, 3H), 7.74 (dd, 1H, *J* = 11.5, *J* = 1.8), 7.80 (ddd, 1H, *J* = 8.5, *J* = 1.8, *J* = 0.9), 8.20 (dd, 1H, *J* = 8.1, *J* = 8.1); ^{13}C NMR (CD_3OD, 100 MHz) δ 24.2, 117.3 (d, 21.1), 123.6, 127.1 (d, 3.1), 128.2, 132.2 (d, 11.3), 153.8 (d, 243.9), 167.8 (d, 2.6), 171.5; ^{19}F NMR (CD_3OD, 376 MHz) δ -128.6

Synthesis of benzyl 3-fluoro-4-hydroxybenzoate (RA-1): A mixture of benzylbromide (171 mg 1 mmol), 3-fluoro-4-hydroxybenzoic acid (156 mg, 1.0 mmol) and $NaHCO_3$ sodium (101 mg, 1.2 mmol) in anhydrous DMF (15 ml) under an

argon atmosphere was heated at 105ºC under argon atmosphere overnight. The mixture was cooled and then was added saturated aqueous $NaHCO_3$ (7 ml), saturated aqueous NaCl (10 ml) and AcOEt (50 ml). It was filtered through a pad of Celite® and after decantation the aqueous layer was extracted with AcOEt (2×20 ml). The combined organic layers were dried over anhydrous $MgSO_4$ and concentrated in vacuo. Finally the crude product was purified by silica gel column chromatography (eluent: AcOEt/hexane, 1:3) to afford 147 mg (60%) of compound **RA-1** as a white solid. M.p. 93–94 °C; IR (KBr): wavenumber (ν_{max}) = 3330, 1684, 1621, 1592, 1522; ^{1}H NMR ($CDCl_3$, 400MHz) δ 5.35 (s, 2H), 6.20 (bs, 1H), 7.00-7.07 (m, 1H), 7.32-7.48 (m, 5H), 7.78-7.83 (m, 2H); ^{13}C NMR ($CDCl_3$, 100 MHz) δ 66.9, 117.0 (d, *J* = 2.0), 117.2 (d, *J* = 19.6), 122.9 (d, *J* = 6.0), 127.2 (d, *J* = 3.2), 128.2, 128.3, 128.6, 135.8, 148.2 (d, *J* = 14.2), 150.4 (d, *J* = 237.6), 165.5 (d, *J* = 2.8); ^{19}F NMR ($CDCl_3$, 376 MHz) δ -139.7; HRMS (ESI+): calculated for $C_{14}H_{11}FNaO_3$ $[M+Na]^+$ 269.0584; found 269.0559

General procedure for the synthesis of bis 3-fluoro-4-hydroxybenzoates from dibromomethylbenzene derivatives: A mixture of the corresponding dibromide derivate (1.0 mmol), 3-fluoro-4-hydroxybenzoic acid (343 mg, 2.2 mmol) and $NaHCO_3$ (210 mg, 2.5 mmol) in anhydrous DMF (15 mL) under an argon atmosphere was heated at 105ºC overnight. The mixture was cooled and then was added saturated aqueous $NaHCO_3$ (7 ml), saturated aqueous NaCl (10 ml) and AcOEt (50 ml). It was filtered through a pad of Celite® and after decantation the aqueous layer was extracted with AcOEt (2×20 ml). The combined organic layers were dried over anhydrous $MgSO_4$ and concentrated in vacuo. Finally the crude product was purified by silica gel column chromatography (eluent: AcOEt/hexane, 1:3).

1,3-phenylenebis(methylene) bis(3-fluoro-4-hydroxybenzoate) (RA-2): Application of general procedure to 1,3-bis(bromomethyl)benzene and 3-fluoro-4-hydroxybenzoic acid afforded 145 mg (35%) of compound **RA-2** as a white solid. M.p. 165–166 °C; IR (KBr): ν_{max} = 3250, 1700, 1616, 1597, 1517; ^{1}H NMR (CD_3OD, 400MHz) δ 5.27 (s, 4H), 6.85-6.95 (m, 2H), 7.34-7.35 (m, 3H), 7.46 (bs, 1H), 7.60-7.70 (m, 4H); ^{13}C NMR (CD_3OD, 100 MHz) δ 67.3, 118.3 (d, *J* = 20.0), 118.4 (d, *J* = 3.0), 122.6 (d, *J* = 6.0), 127.9 (d, *J* = 3.0), 128.6, 128.8, 129.9, 138.1, 151.3 (d, *J* = 12.9), 152.2 (d, *J* = 240.3), 166.8 (d, *J* = 2.7); ^{19}F NMR (CD_3OD, 376 MHz) δ -138.7; HRMS (ESI+): calculated for $C_{22}H_{16}F_2NaO_6$ $[M+Na]^+$ 437.0807; found 437.0787

1,2-phenylenebis(methylene) bis(3-fluoro-4-hydroxybenzoate) (RA-3): Application of general procedure to 1,2-bis(bromomethyl)benzene and 3-fluoro-4-hydroxybenzoic acid afforded 156 mg (38%) of compound **RA-3** as a white solid. M.p. 207–208 °C; IR (KBr): ν_{max} = 3281, 1703, 1619, 1523; ^{1}H NMR (CD_3OD, 400MHz) δ 5.45 (s, 4H), 6.80-6.90 (m, 2H), 7.35-7.45 (m, 2H), 7.48-7.53 (m, 2H), 7.54-7.60 (m, 4H); ^{13}C NMR (CD_3OD, 100 MHz) δ 65.5, 118.2 (d, *J* = 20.0), 118.4 (d, *J* = 3.0), 122.5 (d, *J* = 6.0), 127.9 (d, *J* = 3.0), 130.0, 131.4, 136.3, 151.5 (d, *J* = 12.9), 152.2 (d, *J* = 240.3), 166.8 (d, *J* = 2.7); ^{19}F NMR (CD_3OD, 376 MHz) δ -138.6; HRMS (ESI+): calculated for $C_{22}H_{16}F_2NaO_6$ $[M+Na]^+$ 437.0807; found 437.0809

1,4-phenylenebis(methylene) bis(3-fluoro-4-hydroxybenzoate) (RA-4): Application of general procedure to 1,4-bis(bromomethyl)benzene and 3-fluoro-4-hydroxybenzoic acid afforded 138 mg (33%) of compound **RA-4** as a white solid. M.p. 212–213 °C; IR (KBr): ν_{max} = 3269, 1684, 1617, 1600, 1530; ^{1}H NMR (CD_3OD, 400 MHz) δ 5.27 (s, 4H), 6.90-6.95 (m, 2H), 7.41 (s, 4H), 7.60-7.70 (m, 4H); ^{13}C NMR (CD_3OD, 100 MHz) δ 67.3, 118.3 (d, *J* = 19.9), 118.5 (d, *J* = 3.0), 122.6 (d, *J* = 6.0), 127.9 (d, *J* = 3.0), 129.4, 137.6, 151.4 (d, *J* = 12.8), 152.3 (d, *J* = 240.3), 166.9 (d, *J* = 2.6); ^{19}F

NMR (CD_3OD, 376 MHz) δ -138.5; HRMS (ESI+): calculated for $C_{22}H_{16}F_2NaO_6$ $[M+Na]^+$ 437.0807; found 437.0807

5-(hydroxymethyl)-1,3-phenylene)bis(methylene) bis(3-fluoro-4-hydroxybenzoate (RA-6): Application of general procedure for the synthesis of esters from bromide derivatives to 1,3-bis(bromomethyl)-5-hydroxymethylbenzene and 3-fluoro-4-hydroxybenzoic acid afforded 125 mg (28%) of compound **RA-6** as a white solid. ^1H NMR (CD_3OD, 400MHz) δ 4.63 (s, 2H), 5.31 (s, 4H), 6.90-6.95 (m, 2H), 7.38-7.42 (m, 3H), 7.60-7.70 (m, 4H); ^{13}C NMR (CD_3OD, 100 MHz) δ 64.8, 67.4, 118.3 (d, *J* = 20.0), 118.5 (d, *J* = 3.0), 122.7 (d, *J* = 6.0), 127.4, 127.5, 128.0 (d, *J* = 3.0), 138.3, 143.8, 151.4 (d, *J* = 12.8), 152.3 (d, *J* = 240.3), 166.8 (d, *J* = 2.7); ^{19}F NMR (CD_3OD, 376 MHz) δ -138.5

Synthesis of 1,3-phenylenebis(methylene) bis(4-acetamido-3-fluorobenzoate) (RA-5): A mixture of 1,3-bis(bromomethyl)benzene (132 mg, 0.5 mmol), 4-acetamido-3-fluorobenzoic acid (217 mg, 1.1 mmol) and K_2CO_3 (173 mg, 1.25 mmol) in anhydrous DMF (7 ml) under an argon atmosphere was heated at 105ºC overnight. The mixture was cooled and then saturated aqueous $NaHCO_3$ (3 ml), saturated aqueous NaCl (5 ml) and AcOEt (25 ml) were added. The obtained mixture was filtered through a pad of Celite® and after decantation the aqueous layer was extracted with AcOEt (2×10 ml). The combined organic layers were dried over anhydrous $MgSO_4$ and concentrated in vacuo. Recrystallization from methanol afforded 123 mg (50%) of the compound **RA-5** as a brownish solid. M.p. 190–191 °C; IR (KBr): ν_{max} = 3305, 3262, 3192, 1719, 1676, 1620, 1607, 1541; ^1H NMR (CD_3OD, 400MHz) δ 2.14 (s, 6H), 5.36 (s, 4H), 7.42-7.45 (m, 3H), 7.56 (bs, 1H), 7.70-7.80 (m, 4H), 8.23 (dd, 2H, *J* = 8.1, *J* = 8.1), 10.03 (bs, 2H); ^{13}C NMR (CD_3OD, 100 MHz) δ 23.7, 66.0, 115.9 (d, *J* = 21.2), 122.2, 124.9 (d, *J* = 6.9), 125.8 (d, *J* = 2.9), 127.2, 127.6, 128.7,

131.3 (d, *J* = 11.1), 136.3, 151.8 (d, *J* = 244.1), 164.2 (d, *J* = 2.5), 169.2; ^{19}F NMR (CD_3OD, 376 MHz) δ -124.7; HRMS (ESI+) (from DMF solution): calculated for $C_{26}H_{22}F_2N_2NaO_6$ $[M+Na]^+$ 519.1338; found 519.1307

Cell lines: hKCa3.1-HEK293 cells, a kind gift from Dr. Khaled M. Houamed, University of Chicago (Cao and Houamed, 1999), hKv1.2-B82 cells (Werkman et al., 1992), mKv1.3-L929 cells (Grissmer et al., 1994), hKv7.4-HEK293 (a kind gift from Nicole Schmitt, University Copenhagen, DK), hERG-HEK293 (a kind gift from Craig January, University of Wisconsin, Madison, WI), hKCa2.1-HEK293 cells and rKCa2.2-HEK293 cells, hKCa2.3-COS7 cells (Sankaranarayanan et al., 2009), 3T3 fibroblasts (3T3-L1, ref# CL-173, ATCC, Rockville, MD), U251 glioblastoma cells, and primary porcine coronary artery endothelial cells (PCAEC), were cultured in DMEM supplemented with 10% FCS and penicillin/streptomycin (all from Biochrom KG, Berlin, Germany). PCAEC were isolated from hearts as described previously (Olivan-Viguera et al., 2013). Hearts were kindly provided by the local abattoir (Mercazaragoza, Zaragoza). Prior to patch-clamp experimentation, cells were trypsinized, seeded on cover slips in a NaCl bath solution (see below), and used for electrophysiological measurements within the same day.

Compounds and chemicals: Compounds for synthesis and experimentation were purchased from Sigma/Aldrich, Tocris, Fluorochem, or Alfa Aesar. TRAM-34 (Wulff et al., 2000) and SKA-31 (Sankaranarayanan et al., 2009) were synthesized in the Wulff laboratory (Pharmacology, UC Davis, CA). Stock solutions (at 1 or 10 mM) of all compounds were prepared with dimethylsulfoxide (DMSO). The final DMSO

concentration did not exceed 0.5% in single experiments testing one or more compounds.

Patch-clamp electrophysiology: Inside-out and whole-cell membrane currents were recorded using an EPC10-USB patch-clamp amplifier (HEKA Electronics, Germany), U-ramps (-100 to 100 mV, 1 sec), and Patchmaster™ software as described in more detail previously (Olivan-Viguera et al., 2013). Amplitudes of K^+-outward currents were measured at 0 mV. For measurements of hERG currents we used a pre-pulse to -80 mV (1 sec), a depolarizing pulse to +30 mV (1 sec), and a pulse to -40 mV (1 sec). Leak subtraction was omitted during data acquisition, although "ohmic" leak was subtracted if appropriate. In *fast* whole-cell experiments on KCa channels, the K-pipette solution was composed of (in mM): 140 KCl, 1 $MgCl_2$, 2 EGTA, 1.71 $CaCl_2$ (1 µM $[Ca^{2+}]_{free}$) and 5 HEPES (adjusted to pH 7.2 with KOH). For measuring Kv channels, the pipette solution contained 100 nM $[Ca^{2+}]_{free}$ (2 mM EGTA, 0.7 mM $CaCl_2$). The NaCl bath solution was composed of (mM): 140 NaCl, 5 KCl, 1 $MgSO_4$, 1 $CaCl_2$, 10 glucose and 10 HEPES (adjusted to pH 7.4 with NaOH). For calculation of IC_{50} values, data points were fitted using the "dose-response" equation: y = A2 + (A1-A2)/(1 + (x/x0)^p) or the Boltzmann equation: y = A2 + (A1-A2)/(1 + exp((x-x0)/dx)). The inside-out experiments on $hK_{Ca}3.1$ shown in Fig. 2D were performed in symmetrical K^+. The extracellular solutions contained (in mM): 154 KCl, 10 HEPES (pH = 7.4), 2 $CaCl_2$, 1 $MgCl_2$. Solutions on the intracellular side contained (in mM): 154 KCl, 10 HEPES (pH = 7.2), 10 EGTA, 1.75 $MgCl_2$ and $CaCl_2$ to yield calculated free Ca^{2+}-concentrations of 0.05, 0.1, 0.25, 0.3, 0.5, 1, 10 and 30 µM. Free Ca^{2+} concentrations were calculated with the *MaxChelator* program assuming a temperature of 25°C, a pH of 7.2 and an ionic strength of 160 mM. Cells were

clamped to a holding potential of at 0 mV and K_{Ca} currents were measured using 200-ms voltage-ramps from -80 to 80 mV applied every 5 sec.

Myography on porcine coronary arteries: Isometric myography on porcine coronary artery rings was done as described in detail previously (Alda et al., 2009; Valero et al., 2011). In brief, rings of arteries were mounted onto an isometric force transducer (Pioden UF1, Graham Bell House, Canterbury, UK). The bath containing Krebs buffer (37°C; equilibrated with 95% O_2/5% CO_2) consisted of (in mM): NaCl 120, $NaHCO_3$ 24.5, $CaCl_2$ 2.4, KCl 4.7, $MgSO_4$ 1.2, KH_2PO_4 1 and glucose 5.6, pH 7.4. Rings were pre-stretched to an initial tension of 1 g (10 mN). Changes in force were registered using a Mac Lab System/8e program (AD Instruments Inc, Milford, MA, USA) at a sample rate of 0.5 sec. To analyze EDH-type relaxation, the buffer contained the NO-synthase blocker, *N*ω-nitro-L-arginine (L-NNA, 300 µM), and the cyclooxygenase blocker, indomethacin (10 µM). Rings were pre-contracted with the vasospasmic thromboxane analogue, U46619 (0.2 µM) in the presence of the RA-2 or its vehicle DMSO, followed by relaxation with BK (1 µM). Thereafter, rings were fully contracted with KCl (60 mM) buffer for 10 min, followed by addition of sodium nitroprusside (10 µM) to produce endothelium-independent relaxation.

Stock solutions of compounds were made in DMSO and appropriate amounts were added to the bath. Other compounds were dissolved in Milli-Q water. Data analysis: Relaxations were determined as % change of pre-contraction and relative to the totally relaxed state (absence of the contracting agent).

Blood pressure telemetry: Telemetry was performed as described previously (Brähler et al., 2009; Radtke et al., 2013). Animal protocols were in accordance with ARRIVE guidelines and approved by the Institutional Animal Care and Use Committee of the University of Zaragoza and IACS (CEA; permit no. PI01/13). In brief, TA11PA-C10 pressure transducers (Data Sciences International (DSI), St Paul, Minnesota, USA) were implanted into the left carotid artery of 4 adult female wt and three adult female KCa3.1-/- (Brähler et al., 2009) under deep anesthesia as described previously (Radtke et al., 2013). Mice were allowed to recover for 10 days until reaching normal day night rhythm. Mice had free access to tap water and standard chow. Telemetry data were recorded over 1 minute every 10 minutes over 24 hrs and averaged. Data were analyzed using the DSI software.

The compound or vehicle (peanut oil) was injected during the 3rd hr of the dark phase (activity phase) and we collected telemetry data after 20-30 min after injection. To minimize stress and pain caused by i.p. injections, mice were briefly anesthetized by isoflurane inhalation.

After a first injection, animals were re-used for injections of a higher dose of RA-2 or vehicle.

Preparation and injection of RA-2: Appropriate amounts of RA-2 were dissolved in warmed peanut oil (Sigma-Aldrich) to give a dose of 3, 30, or 100 mg/kg. Injection volume was ≤ 600 □l.

Pharmacokinetics: RA-2 was dissolved in peanut oil and 30 mg/kg were administered i.p. to female C57Bl6J mice (20-30 g, 3-5 month old), n=3 per time point) as described above. Mice were sacrificed at 1, 2, 4, 8, 24, or 48 hours after injection. Blood was taken by puncture of the right ventricle under CO_2 anesthesia

(permit no. PI01/13), transferred into EDTA-containing tubes, and stored on ice until further processing. EDTA-blood was centrifuged at 1,000 g for 10 min and 4°C and plasma was stored at -20°C supernatant. Tissue samples (liver, brain, and femoral skeletal muscle) were excised, frozen, and stored at -20°C until use.

Plasma (50 µl) was added to 950 µl acetonitrile, vortexed and centrifuged at 13,500 g for 30 minutes at room temperature to precipitate the protein. The supernatant was transferred to a 4 ml vial, concentrated to dryness and reconstituted with acetonitrile to 150 µl. Tissue samples (200 mg) were homogenized in 1 ml of H_2O with a Brinkman Kinematica PT 1600E homogenizer and protein precipitated with 1 ml of acetonitrile. The samples were then centrifuged at 13,500 g for 30 minutes. The supernatants was concentrated to dryness and reconstituted in 200 µl of acetonitrile. LC/MS analysis was performed with a Waters Acquity UPLC (Waters, New York, NY) equipped with a Acquity UPLC BEH 1.7 µm RP-8, 2.1 X 150 mm column (Waters, New York, NY) interfaced to a TSQ Quantum Access Max mass spectrometer (MS) (ThermoFisher Scientific, Waltham, MA, USA). Using atmospheric pressure chemical ionization (APCI) MS and selective reaction monitoring (SRM) (capillary temperature 327 °C, vaporization temperature 350°C, collision energy 38eV, negative ion mode), RA-2 was quantified by its base peak of 110.2 m/z and its concentration was calculated with a 4-point calibration curve from 10 nM to 1 µM. The mobile phase consisted of acetonitrile and water, both containing 0.2% acetic acid with a flow rate of 0.300 ml/min. The gradient was ramped from 95/5 water/acetonitrile to 5/95 acetonitrile/water over 2 minutes and returned to 95/5 water/acetonitrile after 6 minutes. RA-2 was introduced onto the column with an injection volume of 6 µl. Using these conditions, RA-2 had a retention time (RT) of 3.78 min. Liver metabolites were analyzed under full scan mode without collision

energy with a mass range of 150–1500 m/z. The mobile phase consisted of an isocratic gradient (90/10 acetonitrile/water). Under these conditions, RA-2 had a retention time of 1.76 min and liver metabolites eluted at 1.74, 2.71, 3.11 minutes.

Statistics: Data are given as mean ± SEM if not stated otherwise. For comparison of datasets we used the unpaired Student's t-test or one-way ANOVA followed by the Tukey-post hoc test in the case of multiple comparison. *P*-values of <0.05 were considered significant.

Results:

We previously identified 13b (Figure 1 A) as a negative-gating modulator of KCa2/3 channels (Olivan-Viguera et al., 2013). However, 13b´s druglikeness is poor because of its high molecular weight and high lipophilicity, limiting its *in vivo* bioavailability. We therefore synthesized a series of smaller and less lipophilic mono- and di-benzoates that met *Lipinski's rule of five* for a drug-like compound (Lipinski et al., 2001) (Scheme 1 in Figure 1 B). RA-1, RA-2, RA-3, RA-4, and RA-6 (Figure 1 B) were obtained from the corresponding mono- or dibromide- 3-fluoro-4-hydroxybenzoic acid. RA-5 was obtained from 1,3-bis(bromomethyl)benzene and 4-acetamido-3-fluorobenzoic acid, which in turn was obtained by acetylation of 4-amino-3-fluorobenzoic acid.

Electrophysiology

We performed inside-out and whole-cell patch-clamp experiments on cloned hKCa3.1 and hKCa2.3 as well as native KCa3.1/KCa2 in porcine coronary artery endothelial cells (PCAEC) and a series of distantly related K channels to test efficacy and selectivity.

Removal of lipophilic branches from the parent compound led to the following results: Compound RA-1 with only one benzoate ring had no considerable inhibitory activity on KCa3.1 (Table 1). The 1,3-dibenzoate RA-2 was a potent KCa3.1 and KCa2.3 inhibitor with IC_{50}s of 17 ± 3 nM and 2 ± 1 nM as determined in inside-out recordings on hKCa3.1 in HEK-293 cells and hKCa2.3 in COS7 cells (Figure 2 A and B, see Table 1 and Table S1 for numeric data). RA-2 similarly inhibited cloned hKCa2.1 and rKCa2.2 at nanomolar concentrations (Table S1). We obtained similar IC_{50} values in whole-cell experiments on murine KCa3.1 expressed in 3T3-fibroblasts

(Figure S1 A). The 1,2- and 1,4-dibenzoate derivatives, RA-3 and RA-4 showed a similar potency with an IC_{50} for RA-3 of 6 ± 2 nM (Table 1; Figure S1 B). Compound RA-5, in which the hydroxyl group on the benzoic acid moiety has been substituted by an acetamido group (Figure 1 B), had no considerable inhibitory activity (Table 1). Introduction of a hydroxymethyl substituent in 5 position of the central aromatic core (RA-6, Figure 1 B) led to a loss of activity (Table 1). It is noteworthy, that 3-fluorobenzoic moieties (4-hydroxy-3-fluorobenzoic acid and 4-amino-3-fluorobenzoic acid) and 1,3-phenylenedimethanol as potential metabolites of RA-2/RA-5 hydrolysis, respectively, did not modify KCa3.1 currents.

Similar to our previous observations with the template 13b (Olivan-Viguera et al., 2013), we found that the positive-gating modulator, SKA-31, was capable of reversing the inhibition caused by nanomolar but not micromolar concentrations of RA-2 (Figure 2 C). This suggested 1) antagonism of the two compounds, 2) inhibitory actions of RA-2 similar to that of 13b, and 3) that RA-2 acted as a negative-gating modulator again similar to 13b (Olivan-Viguera et al., 2013).

To determine if the effects of RA-2 were Ca^{2+}-dependent as was the case with previously described negative-gating modulators like NS8593 and its derivatives (Jenkins et al., 2011), we performed inside-out experiments, in which we varied the intracellular $[Ca^{2+}]_i$ concentration and investigated the ability of 100 nM of RA-2 to inhibit KCa3.1 currents. As shown in Figure 2D, 100 nM of RA-2 nearly completely inhibited the current elicited by 500 nM $[Ca^{2+}]_i$, while the same concentration had a smaller effect in the presence of saturating 30 μM $[Ca^{2+}]_i$. Ca^{2+}-concentration response curves obtained in the presence and absence of 100 nM of RA-2 (Figure 2D, on right) revealed that RA-2 shifted the curve to the right but also reduced the

maximal current at 30 μM, suggesting that the compound exerted negative-gating modulating of KCa3.1.

In respect to selectivity, we found that RA-2 had no considerable inhibitory or activating effects at a concentration of 1 μM on the distantly related human KCa1.1 channel in U251 glioblastoma cells, cloned Kv1.2, Kv1.3, Kv7.4 channels, the important cardiac hERG channels (Kv11.1), or native K_{IR} channels in U251 cells. The data are summarized in supplemental table S1.

Patch-clamp on porcine coronary endothelium and isometric myography

Considering RA-2 one of the drug-like compounds of this series, we continued evaluating functional activity in an *ex vivo* test system, i.e. porcine coronary arteries (Olivan-Viguera et al., 2013), in which KCa2/3 channels have been suggested to initiate –at least in part (Ge et al., 2000)- the so-called endothelium-derived hyperpolarization (EDH)-type of endothelium-dependent vasorelaxation (Edwards et al., 2010). In the present study, we first measured endogenous KCa2 and KCa3.1 currents in freshly isolated PCAEC and we found that 1 μM RA-2 virtually abolished SKA-31-activated composite KCa2/KCa3.1 currents and also fully inhibited the TRAM-34–insensitive KCa2-mediated current in these cells (Figure 3 A).

Our isometric myography experiments in the presence of blockers of NO and prostacyclin synthesis (to specifically study EDH-type relaxation) showed that RA-2 at 1 μM did not modulate basal tone in these arteries (not shown). However, RA-2 almost abolished the bradykinin-induced relaxation in rings being strongly pre-contracted with a vasospasmic agent, the thromboxane analogue, U46619 (Figure 3 B). RA-2 did not modulate SNP-induced and endothelium-independent relaxation of 60 mM-KCl-contracted rings (data not shown).

Taken together, RA-2 showed activity in porcine coronary arteries by inhibiting EDH-type endothelium-dependent relaxation.

Systemic cardiovascular effects of RA-2

In keeping with the expression of KCa3.1 and KCa2.3 channels in the vascular endothelium and their proposed roles in systemic cardiovascular regulation (Brähler et al., 2009), we next evaluated cardiovascular activity and selectivity of the pan-KCa2/3-negative-gating modulator, RA-2, by blood pressure telemetry in wt and KCa3.1-/- mice (Brähler et al., 2009). If compared to vehicle, i.p. injections of 3, 30, or 100 mg/kg RA-2 did not significantly change mean arterial blood pressure (MAP) over 24 hrs in the wt mice (Figure 4 A, for 30 mg/kg, and Suppl. Figure S3 A, for 3 and 100 mg/kg). However, RA-2 at 30 and 100 mg/kg significantly reduced heart rate (HR). The reduction in heart rate started apparently 30-60 min after injection and reached lowest levels (≈Δ145 bpm) at the end of the activity phase and during the resting phase (Figure 4 B and Figure S3 A, lower panel on right). RA-2 at the lower dose of 3 mg/kg produced a smaller reduction in HR (Figure S3 A, lower panel on left).

Besides the lower HR, waveforms were similar in the presence or absence of RA-2 and are shown in Figure S3 B.

We next evaluated to which extent the HR reducing effects of RA-2 in the wt mice depended on KCa3.1 channels and performed telemetry in KCa3.1-/- mice. Similar to wt mice, RA-2 at 30 mg/kg did not change MAP in the KCa3.1-/- mice (Figure 4 C, on left). However, we did not find a reduction in HR in KCa3.1-/- mice ($P<0.05$; Figure 4 D, on right).

Together, the telemetric monitoring revealed that RA-2 had no gross deleterious effects on blood pressure. Nonetheless, it is noteworthy that RA-2 reduced HR in a KCa3.1–dependent manner.

Pharmacokinetics of RA-2

Analysis of tissue concentrations and distribution of RA-2 in plasma, brain, skeletal muscle, fat and liver by a combination of ultra-high performance liquid chromatography and mass spectrometry (Figure 5A) revealed that RA-2 plasma concentration was 136 nM at 1 hour after injection, 18 nM at 2 hours and that the compound was not detectable at later time points (Figure 5B). RA-2 went rapidly into tissue (skeletal muscle, brain and fat) where it reached at 1 h concentrations of 1.7 µM (skeletal muscle), 91 nM (brain) and 6 µM (fat) (Figure 5C and 5D). As expected for an ester, RA-2 was rapidly cleared from the circulating blood within 1 h (Figure 5B) presumably via hydrolysis by plasma and hepatic esterases as indicated by the absence of RA-2 in liver and high amounts of possible metabolites in this tissue (Figure 6). Compounds with the masses shown in Figure 6 were identified in liver homogenate and were present in estimated concentrations of 1 to ~50 µM but could not be precisely quantified without reference compounds. The metabolites were likely eliminated via the bile since metabolites were not detectable in plasma at the same time point.

In conclusion, i.p. administration of RA-2 yielded tissue concentrations above the IC_{50} for channel inhibition for 1-2 h that fairly corresponded to the beginning of bradycardia (Figure 4).

Discussion

The purpose of the present study was to synthesize potent and structurally novel pharmacophores for negative-gating modulation of KCa2/3 channels. We succeeded in identifying three fluoro-di benzoates that inhibited KCa2/3 channels in the low nanomolar range and in a Ca^{2+}-concentration-dependent manner and exhibited antagonism with a positive gating modulator. The most drug-like compound RA-2 inhibited KCa2/3-initiated EDH-type relaxation and *in vivo* treatments did not show acute toxicity, although we found a KCa3.1-dependent reduction of heart rate.

Compared to 13b (Lamoral-Theys et al., 2010) that served as a template for structural modifications, compounds RA-2, RA-3 and RA-4, in which two of the three 3-fluoro-4-hydroxybenzoyloxymethyl substituents in 13b were conserved, showed inhibitory activity. RA-2 with both substituents in 1,3 position was equally potent in inhibiting KCa3.1 (RA-2: 17 nM *vs*. 13b: 19 nM (Olivan-Viguera et al., 2013)). In line with the notion that RA-2 is a pan-negative KCa2/3 modulator, all three subtypes of KCa2 channels were inhibited by RA-2 at nanomolar concentrations, although the IC_{50} was higher for RA-2 (2 nM) than for 13b (360 pM) in the case of hKCa2.3. The structurally very similar compounds RA-3 and RA-4 with both substituents in 1,2 and 1,4- position, respectively, were also found to be potent KCa3.1 inhibitors. A major change in the structure such as the absence of an additional 3-fluoro-4-hydroxybenzoyloxymethyl substituent, as in RA-1, the substitution of the hydroxyl groups by acetamido groups on the benzoic acid moieties, as in RA-5, or the introduction of a hydroxymethyl substituent in 5 position on the central aromatic core, as in RA-6, gave lower logP values but caused a loss of inhibitory efficacy. Thus regarding SAR, this suggested that the intactness of the aromatic core as lipophilic

spacer and the presence of at least two 3-fluoro-4-hydroxybenzoyloxymethyl branches were critical for maintaining inhibitory efficacy. A change in the relative position of the two 3-fluoro-4-hydroxybenzoyloxymethyl branches had no major consequences with LogP values (4.7) similar to RA-2.

Together, the three structurally similar compounds, RA-2, RA-3, and RA-4 were identified as potential pharmacophores for pan-negative-modulating of KCa2/3 channels that had a better chemical profile with a lower MW of 414 Da (RA-2, RA-3, RA-4) and lower LogP values of 4.7 than the starting compound 13b (MW 582; LogP 6.0), suggesting *in vivo* utility.

Similar to 13b, RA-2 acted as a negative-gating modulator as concluded from the substantially more potent inhibition at nanomolar Ca^{2+} and the antagonism (relief of channel inhibition) by the positive-gating modulator, SKA-31. Structurally, the negative-gating modulation by RA-2 and its antagonism by the positive gating modulator, SKA-31, could occur at the interface of calmodulin (CAM) and the cytosolic C-terminal calmodulin-binding domain (CAMBD) of the channels. Indeed, docking experiments using co-crystals of CAM and the c-terminal CAMBD of KCa2.2 (Zhang et al., 2012) revealed that NS309 and EBIO that are structurally related to SKA-31 bind in the interface between the CAM and the CAMBD to keep the channel in the open state. However, we do not wish to exclude that other allosteric effects may account for the functional antagonism observed here.

Regarding selectivity, micromolar concentrations of RA-2 did not interfere (block or activate) with a series of members of distantly related K^+ channel families, suggesting considerable selectivity for KCa2/3 over other K^+ channels.

The utility of RA-2 as a new tool and/or drug candidate for *in vivo* use was demonstrated by the results of the present *ex vivo* and *in vivo* experiments on freshly isolated PCAEC and coronary arteries. The patch-clamp experiments showed that endogenous KCa2 and KCa3.1 currents in PCAEC were fully inhibited by RA-2, in this regard similar to 13b. The results from myography on porcine coronary arteries showed that similar to 13b (Olivan-Viguera et al., 2013) RA-2 did not modulate basal tone, suggesting that KCa2/3 channels were not essentially involved in the control of basal arterial tone at least under these *ex vivo* conditions. Agonist-induced EDH-type relaxations independent of nitric oxide are known to require the activation of KCa2/3 channels and subsequent smooth muscle hyperpolarization in many vascular beds (Edwards et al., 2010). Here we found that RA-2 inhibited bradykinin-induced EDH-type relaxation in the presence of the vasospasmic agent, U46619. This inhibition was almost complete and the small RA-2-resistant relaxation could be explained by the contribution of other endothelium-derived relaxing factors such as eicosanoids as shown previously (Fisslthaler et al., 1999). Nonetheless, these results showed that KCa2/3 activation by bradykinin-induced endothelial stimulation was a critically step in EDH-type relaxation in strongly pre-contracted porcine coronary artery as also suggested previously by others (Ge et al., 2000). However, the specific contributions of KCa2/3 to this response were not elucidated so far. Regarding the potency of inhibition by RA-2, it was noteworthy that RA-2 was more efficient than the more lipophilic template 13b that did not produce significant inhibition of bradykinin-induced relaxation of porcine coronary arteries in the presence of the vasospamic U46619 in our previous study (Olivan-Viguera et al., 2013).

Our telemetry in freely moving mice showed that the animals tolerated the RA-2 injections well at a dosage of up to 100 mg/kg/d (highest dose tested). There were no signs of acute toxicity. Alterations of arterial pressure were not evident and, therefore, acute systemic KCa2/3 inhibition by RA-2 appeared to be safe. However, it should be noted that RA-2 was cleared from the circulation rapidly, presumably via hydrolysis by plasma and hepatic esterases. Nonetheless, RA-2 entered the brain and skeletal muscle where tissue concentrations reached values clearly above IC_{50} values within the first 2 hours after administration.

Albeit blood pressure changes were not evident, a single dose RA-2 (30 or 100 mg/kg) produced an appreciable decrease in heart rate, which was apparent after injection and more pronounced during the end of the activity phase and the resting phase (≈Δ145 bpm). An obvious interpretation of these data is that this bradycardia might be an adaptation to an increase of total peripheral resistance - caused by endothelial KCa2/KCa3 inhibition in resistance size-arteries - and baroreceptor activation to lower cardiac output and to maintain pressure constant.

In addition to expression in neurons and arteries, expression of KCa2 channels, in particular of the KCa2.2 subtype, have been reported in atrial myocytes (Li et al., 2009; Tuteja et al., 2005) and the atrioventricular node (Zhang et al., 2008). Indeed, blockers of KCa2 have been suggested to serve as antiarrhythmic drugs by prolonging repolarization times and thereby action potential duration, finally terminating atrial fibrillation (Diness et al., 2010). Thus, one alternative explanation for the lower heart rate might be that cardiac KCa2 inhibition by RA-2 caused prolongation of action potential duration in atrial tissues. An additional explanation could be that RA-2 altered transmission time at the level of the atrioventricular node.

Nonetheless, the precise mechanisms, by which RA-2 produced bradycardia, remains to be identified in future studies. At present we do not wish to exclude that by esterase-mediated hydrolysis RA-2 could be a source of di-phenols with potential anti-oxidative properties. However, the observation that RA-2-induced bradycardia was not seen in KCa3.1-deficient mice suggested that an inhibition of KCa3.1 channels but not of KCa2 channels was mechanistically involved in the wild type-situation.

In conclusion, we identified RA-2 as a selective pan-negative-gating modulator of KCa2/3 channels with nanomolar potency and *ex vivo* and *in vivo* activity in coronary arteries endothelium and in systemic cardiovascular regulation. We supposed RA-2 as a novel pan-negative-gating modulator of KCa2/3 channels with a drug-like profile. Moreover, RA-2 can be considered a useful tool compound to study physiological and pathophysiological roles of KCa2/3 channels *in vitro* or *in vivo* and may be of therapeutic utility to treat hypotension and undesired hyperemia as well as chronic inflammation and disorders characterized by abnormal cell proliferation.

Disclosures and competing interests:

None

Acknowledgements: AOV and RK were supported by the Deutsche Forschungsgemeinschaft (KO1899/11-1 to RK), European Community (FP7-PEOPLE Project 321721), the Danish Hjerteforening, Department of Industry & Innovation, Government of Aragon (GIPASC-B105), and the Fondo de Investigación

Sanitaria (Red HERACLES RD12/0042/0014). JAG, MDD and RB were supported from the Government of Aragón (GA E-102). BMB was supported by a NIGMS-funded Pharmacology Training Program (T32GM099608). NC was supported by a NIHLB-funded Training Program in Basic and Translational Cardiovascular Science [T32HL086350]. HW was supported by the National Institute of Neurological Disorders and Stroke (NINDS), Grant Number R21NS072585. We wish to thank Dr. Eduardo Romanos-Alfonso and Susana Murillo-Pola of the Unit of Functional Evaluations of the IACS for excellent technical support (telemetry).

Authorship Contributions: Participated in research design: Aida Oliván-Viguera, Heike Wulff, Marta Sofia Valero, José A. Gálvez, María D. Díaz-de-Villegas, Ramón Badorrey, Ralf Köhler.

Conducted experiments: Aida Oliván-Viguera, Marta Sofia Valero, Nichole Coleman, Brandon M. Brown, Ramón Badorrey, Ralf Köhler.

Performed data analysis: Aida Oliván-Viguera, Marta Sofia Valero, Nichole Coleman, Brandon M. Brown, Ramón Badorrey, Ralf Köhler.

Wrote or contributed to the writing of the manuscript:

Aida Oliván-Viguera, José A. Gálvez, María D. Díaz-de-Villegas, Heike Wulff, Ramón Badorrey, Ralf Köhler.

1 **Table 1: Inhibitory efficacy of mono- and di-fluorobenzoates on hKCa3.1**

Compound	IC_{50}	% of control at		
		1 μM	5 μM	10 μM
4-amino-3-fluorobenzoic acid		NT	NT	90 ± 3
4-hydroxy-3-fluorobenzoic acid		NT	NT	80 ± 8
1,3-phenylenedimethanol		NT	NT	106 ± 8
RA-1 (**benzyl 3-fluoro-4-hydroxybenzoate**)		94 ± 1	87 ± 2	NT
RA-2 (**1,3-phenylenebis(methylene) bis(3-fluoro-4-hydroxybenzoate**)	17 ± 3 nM	4 ± 1	NT	NT
RA-3 (**1,2-phenylenebis(methylene) bis(3-fluoro-4-hydroxybenzoate**)	6 ± 2 nM	12 ± 2	2 ± 1	NT
RA-4 (**1,4-phenylenebis(methylene) bis(3-fluoro-4-hydroxybenzoate**))		15 ± 6	NT	NT
RA-5 (**1,3-phenylenebis(methylene) bis(4-acetamido-3-fluorobenzoate**)		97 ± 2	94 ± 1	NT
RA-6 (**5-(hydroxymethyl)-1,3-phenylene)bis(methylene) bis(3-fluoro-4-hydroxybenzoate**)		83 ± 3	74 ± 11	NT

Data derived from inside-out patch-clamp experiments on hKCa3.1 stably expressed in HEK293 cells. NT, not tested; data are given as mean ± SEM, $n \geq 3$.

2

3

Table S1: Effects of RA-2 on other K^+ channels

Compound	% of control at		
	100 nM	1 μM	5μM
hKCa2.3* (in COS7)			
RA-2	38 ± 2	21 ± 3	3 ± 1
RA-3	68 ± 4	36 ± 5	11 ± 1
RA-4	71 ± 5	45 ± 12	NT
hKCa2.1 (in HEK293)			
RA-2	61 ± 4	4 ± 2	NT
rKCa2.2 (in HEK293)			
RA-2	41 ± 6	10 ± 1	3 ± 1
hKCa1.1 (in U251)			
RA-2	NT	105 ± 10	NT
hKv1.2 (in B82)			
RA-2	NT	94 ± 4	NT
rKv1.3 (in L929)			
RA-2	NT	93 ± 14	NT
hKv7.4 (in HEK293)			
RA-2	NT	98 ± 7	NT
hERG (in HEK293)			
RA-2	NT	99 ± 2	NT
hK_{IR} (in U251)			
RA-2	NT	102 ± 10	NT

NT, not tested; data are given as mean ± SEM, n ≥ 3. * data from *inside-out* experimentation on cloned hKCa2.3, the other data derived from *whole-cell* experimentation on cloned or native channels in the respective cell line (name in brackets).

Legends to Figures:

Figure 1: Synthesis, structures, and selected properties of mono- and di-fluoro-benzoates. A) Structure of the parent compound, 13b. B) Scheme of synthesis and structures of RA-1 to RA-6, together with molecular weights and LogP values.

Figure 2: Negative-gating modulation of KCa2/3 channels by RA-2. A) On left: Inside-out patch-clamp experiments showing concentration-dependent inhibition of cloned hKCa3.1. B) On left: Inhibition of cloned hKCa2.3. Right panels (A and B): Concentration-response curves. Data points (mean ± SEM; KCa3.1: n=4-10, experiments for each concentration; KCa2.3: n=2-12, experiments each) were fitted with the Boltzmann equation (A) or the "dose-response" equation (B). C) The positive gating-modulator SKA-31 (1 μM) reversed KCa3.1 channel inhibition at nanomolar (on left) but not at micromolar concentrations of RA-2 (on right). Lower panel: Quantitative data (mean ± SEM; n=3, experiments for each concentration). D) Panels on left: Representative currents from inside-out patches in the presence of 500 nM (top) and 30 μM (bottom) intracellular Ca^{2+} before and after application of 100 nM of RA-2. Panel on right: Ca^{2+}-concentration response curve for $K_{Ca}3.1$ activation measured from inside-out patches in absence or presence of 100 nM RA-2. Currents from individual patches were normalized to the effect of 10 μM Ca^{2+} in the absence of RA-2. Data are mean ± SD (n=3, experiments per data point).

Figure 3: Negative-gating modulation of endogenous KCa3.1 and KCa2.3 channels in porcine endothelium and RA-2-evoked modulation of arterial contraction and relaxation of porcine coronary artery. A) On left: Potentiation of KCa2/KCa3.1 from

pre-activation levels (during infusion of 1 µM Ca^{2+}) by 1 µM SKA-31 followed by current inhibition by 1 µM RA-2. In middle: Partial inhibition of SKA-31-potentiated current by 1 µM TRAM-34 followed by complete inhibition of the TRAM-34-insensitive component by 1 µM RA-2. On right: Summary data. Data points are mean ± SEM (n=3-8, arteries for each compound). *P<0.01 SKA-31 vs. Ctrl (without compounds); #P<0.05; SKA-31 vs. TRAM-34, RA-2, or TRAM-34 and RA-2; Student T test. B) RA-2 inhibited bradykinin (1 µM)-induced relaxation in rings strongly pre-contracted with U46619 (0.2 µM). Data points are mean ± SEM (n=5-6, arteries each); **P<0.01.

Figure 4: Systemic cardiovascular actions of RA-2 in mice. A) Telemetric 24 hrs-measurements of mean arterial blood pressure (MAP) after intraperitoneal injections of 30 mg/kg (n=4, experiments) RA-2 or vehicle (n=6, experiments) into a total of 4 wt mice. B) Heart rate (HR) lowering effects of RA-2. C and D) HR-lowering actions of 30 mg/kg RA-2 (n=3, experiments on 3 mice) were absent in KCa3.1-/- mice. Black and white parts of the y-axis indicate dark and light phases. Arrow indicates time of injection (t=0). Data points are mean ± SEM. Horizontal lines above or below data points indicate statistical significant difference from vehicle; * P<0.05, Student T test.

Figure 5: Pharmacokinetics of RA-2. A) RA-2 plasma calibration curve with concentrations ranging from 10 nM to 1 µM (r^2 = 0.9995). The plasma values were determined by Y = 2.58e5x (n=2). B) RA-2 plasma concentrations following i.p. application of 30 mg/kg (n=3, mice). C) Tissue concentrations 1 h after i.p. administration of RA-2 30 mg/kg (n=3, mice). D) Time course of tissue

concentrations after i.p. administration of RA-2 30 mg/kg (n=3, mice). Data points are mean ± SD.

Figure 6: Possibly metabolites of RA-2 found in liver homogenate. Note that the "parent" compound, RA-2, was not found in the liver.

Suppl. Figure S1: A) Inhibition of native mKCa3.1-whole-cell-currents by RA-2 in murine fibroblast (on left) and concentration-response curve (on right). B) Concentration-response curve for inhibition of hKCa3.1 by RA-3 in inside-out experiments. Data points (mean ± SEM; n=2-6, cells or patches, respectively, for each concentration) were fitted with the Boltzmann equation.

Suppl. Figure S2: Representative whole-cell recordings showing that RA-2 did not inhibit hKCa1.1 in U251 glioblastoma cells, cloned hERG, rKv1.3, hK_{IR} in U251 cells (arrow in the lower panel on right indicates inward-rectifying hK_{IR} currents).

Suppl. Figure S3: A) Mean arterial blood pressure (MAP) and heart rate (HR) after intraperitoneal injections of 3 mg/kg (n=4, experiments) and 100 mg/kg (n=4, experiments) into 4 wt mice. Black and white parts of the y-axis indicate dark and light phases and arrow indicates time of injection (t=0). Data on vehicle have been re-plotted from Figure 4. B) Representative recordings of pulse waves after injection of 30 mg/kg RA-2 or vehicle (Ve) in wt (on left) and in KCa3.1-/- mice (on right). Data points are mean ± SEM; horizontal lines below data points indicate statistical significant difference from vehicle; * $P<0.05$; Student T test.

References:

Adelman JP, Maylie J and Sah P (2012) Small-conductance Ca2+-activated K+ channels: form and function. *Annu Rev Physiol* **74**: 245-269.

Alda JO, Valero MS, Pereboom D, Gros P and Garay RP (2009) Endothelium-independent vasorelaxation by the selective alpha estrogen receptor agonist propyl pyrazole triol in rat aortic smooth muscle. *J Pharm Pharmacol* **61**(5): 641-646.

Ataga KI and Stocker J (2009) Senicapoc (ICA-17043): a potential therapy for the prevention and treatment of hemolysis-associated complications in sickle cell anemia. *Expert Opin Investig Drugs* **18**(2): 231-239.

Brähler S, Kaistha A, Schmidt VJ, Wolfle SE, Busch C, Kaistha BP, Kacik M, Hasenau AL, Grgic I, Si H, Bond CT, Adelman JP, Wulff H, de Wit C, Hoyer J and Köhler R (2009) Genetic deficit of SK3 and IK1 channels disrupts the endothelium-derived hyperpolarizing factor vasodilator pathway and causes hypertension. *Circulation* **119**(17): 2323-2332.

Cao YJ and Houamed KM (1999) Activation of recombinant human SK4 channels by metal cations. *FEBS Lett* **446**(1): 137-141.

Chantome A, Potier-Cartereau M, Clarysse L, Fromont G, Marionneau-Lambot S, Gueguinou M, Pages JC, Collin C, Oullier T, Girault A, Arbion F, Haelters JP, Jaffres PA, Pinault M, Besson P, Joulin V, Bougnoux P and Vandier C (2013) Pivotal role of the lipid Raft SK3-Orai1 complex in human cancer cell migration and bone metastases. *Cancer Res* **73**(15): 4852-4861.

Coleman N, Brown BM, Olivan-Viguera A, Singh V, Olmstead MM, Valero MS, Kohler R and Wulff H (2014) New Positive KCa Channel Gating Modulators with Selectivity for KCa3.1. *Mol Pharmacol*.

D'Alessandro G, Catalano M, Sciaccaluga M, Chece G, Cipriani R, Rosito M, Grimaldi A, Lauro C, Cantore G, Santoro A, Fioretti B, Franciolini F, Wulff H and Limatola C (2013) KCa3.1 channels are involved in the infiltrative behavior of glioblastoma in vivo. *Cell Death Dis* **4**: e773.

Damkjaer M, Nielsen G, Bodendiek S, Staehr M, Gramsbergen JB, de Wit C, Jensen BL, Simonsen U, Bie P, Wulff H and Kohler R (2012) Pharmacological activation of KCa3.1/KCa2.3 channels produces endothelial hyperpolarization and lowers blood pressure in conscious dogs. *Br J Pharmacol* **165**(1): 223-234.

Devor DC, Singh AK, Frizzell RA and Bridges RJ (1996) Modulation of Cl- secretion by benzimidazolones. I. Direct activation of a Ca(2+)-dependent K+ channel. *Am J Physiol* **271**(5 Pt 1): L775-784.

Diez-Barra E, Garcia-Martinez JC, Merino S, del Rey R, Rodriguez-Lopez J, Sanchez-Verdu P and Tejeda J (2001) Synthesis, characterization, and optical response of dipolar and non-dipolar poly(phenylenevinylene) dendrimers. *J Org Chem* **66**(17): 5664-5670.

Diness JG, Sorensen US, Nissen JD, Al-Shahib B, Jespersen T, Grunnet M and Hansen RS (2010) Inhibition of small-conductance Ca2+-activated K+ channels terminates and protects against atrial fibrillation. *Circ Arrhythm Electrophysiol* **3**(4): 380-390.

Edwards G, Feletou M and Weston AH (2010) Endothelium-derived hyperpolarising factors and associated pathways: a synopsis. *Pflugers Arch* **459**(6): 863-879.

Ellinor PT, Lunetta KL, Glazer NL, Pfeufer A, Alonso A, Chung MK, Sinner MF, de Bakker PI, Mueller M, Lubitz SA, Fox E, Darbar D, Smith NL, Smith JD, Schnabel RB, Soliman EZ, Rice KM, Van Wagoner DR, Beckmann BM, van Noord C, Wang K, Ehret GB, Rotter JI, Hazen SL, Steinbeck G, Smith AV, Launer LJ, Harris TB, Makino S, Nelis M, Milan DJ, Perz S, Esko T, Kottgen A, Moebus S, Newton-Cheh C, Li M, Mohlenkamp S, Wang TJ, Kao WH, Vasan RS, Nothen MM, MacRae CA, Stricker BH, Hofman A, Uitterlinden AG, Levy D, Boerwinkle E, Metspalu A, Topol EJ, Chakravarti A, Gudnason V, Psaty BM, Roden DM, Meitinger T, Wichmann HE, Witteman JC, Barnard J, Arking DE, Benjamin EJ, Heckbert SR and Kaab S (2010) Common variants in KCNN3 are associated with lone atrial fibrillation. *Nat Genet* **42**(3): 240-244.

Engbers JD, Anderson D, Asmara H, Rehak R, Mehaffey WH, Hameed S, McKay BE, Kruskic M, Zamponi GW and Turner RW (2012) Intermediate conductance calcium-activated potassium channels modulate summation of parallel fiber input in cerebellar Purkinje cells. *Proc Natl Acad Sci U S A* **109**(7): 2601-2606.

Feletou M, Kohler R and Vanhoutte PM (2010) Endothelium-derived vasoactive factors and hypertension: possible roles in pathogenesis and as treatment targets. *Curr Hypertens Rep* **12**(4): 267-275.

Fisslthaler B, Popp R, Kiss L, Potente M, Harder DR, Fleming I and Busse R (1999) Cytochrome P450 2C is an EDHF synthase in coronary arteries. *Nature* **401**(6752): 493-497.

Ge ZD, Zhang XH, Fung PC and He GW (2000) Endothelium-dependent hyperpolarization and relaxation resistance to N(G)-nitro-L-arginine and indomethacin in coronary circulation. *Cardiovasc Res* **46**(3): 547-556.

Grgic I, Eichler I, Heinau P, Si H, Brakemeier S, Hoyer J and Kohler R (2005) Selective blockade of the intermediate-conductance Ca^{2+}-activated K^+ channel suppresses proliferation of microvascular and macrovascular endothelial cells and angiogenesis in vivo. *Arterioscler Thromb Vasc Biol* **25**(4): 704-709.

Grgic I, Kiss E, Kaistha BP, Busch C, Kloss M, Sautter J, Muller A, Kaistha A, Schmidt C, Raman G, Wulff H, Strutz F, Grone HJ, Kohler R and Hoyer J (2009) Renal fibrosis is attenuated by targeted disruption of KCa3.1 potassium channels. *Proc Natl Acad Sci U S A* **106**(34): 14518-14523.

Grissmer S, Nguyen AN, Aiyar J, Hanson DC, Mather RJ, Gutman GA, Karmilowicz MJ, Auperin DD and Chandy KG (1994) Pharmacological characterization of five cloned voltage-gated K+ channels, types Kv1.1, 1.2, 1.3, 1.5, and 3.1, stably expressed in mammalian cell lines. *Mol Pharmacol* **45**(6): 1227-1234.

Hougaard C, Hammami S, Eriksen BL, Sorensen US, Jensen ML, Strobaek D and Christophersen P (2012) Evidence for a common pharmacological interaction site on K(Ca)2 channels providing both selective activation and selective inhibition of the human K(Ca)2.1 subtype. *Mol Pharmacol* **81**(2): 210-219.

Ishii TM, Silvia C, Hirschberg B, Bond CT, Adelman JP and Maylie J (1997) A human intermediate conductance calcium-activated potassium channel. *Proc Natl Acad Sci U S A* **94**(21): 11651-11656.

Jenkins DP, Strobaek D, Hougaard C, Jensen ML, Hummel R, Sorensen US, Christophersen P and Wulff H (2011) Negative gating modulation by (R)-N-(benzimidazol-2-yl)-1,2,3,4-tetrahydro-1-naphthylamine (NS8593) depends on residues in the inner pore vestibule: pharmacological evidence of deep-pore gating of K(Ca)2 channels. *Mol Pharmacol* **79**(6): 899-909.

Kaushal V, Koeberle PD, Wang Y and Schlichter LC (2007) The Ca2+-activated K+ channel KCNN4/KCa3.1 contributes to microglia activation and nitric oxide-dependent neurodegeneration. *J Neurosci* **27**(1): 234-244.

Köhler M, Hirschberg B, Bond CT, Kinzie JM, Marrion NV, Maylie J and Adelman JP (1996) Small-conductance, calcium-activated potassium channels from mammalian brain. *Science* **273**(5282): 1709-1714.

Köhler R, Degenhardt C, Kuhn M, Runkel N, Paul M and Hoyer J (2000) Expression and function of endothelial Ca^{2+}-activated K^+ channels in human mesenteric artery: A single-cell reverse transcriptase-polymerase chain reaction and electrophysiological study in situ. *Circ Res* **87**(6): 496-503.

Köhler R, Kaistha BP and Wulff H (2010) Vascular KCa-channels as therapeutic targets in hypertension and restenosis disease. *Expert Opin Ther Targets* **14**(2): 143-155.

Köhler R, Wulff H, Eichler I, Kneifel M, Neumann D, Knorr A, Grgic I, Kampfe D, Si H, Wibawa J, Real R, Borner K, Brakemeier S, Orzechowski HD, Reusch HP, Paul M, Chandy KG and Hoyer J (2003) Blockade of the intermediate-conductance calcium-activated potassium channel as a new therapeutic strategy for restenosis. *Circulation* **108**(9): 1119-1125.

Lam J, Coleman N, Garing AL and Wulff H (2013) The therapeutic potential of small-conductance KCa2 channels in neurodegenerative and psychiatric diseases. *Expert Opin Ther Targets* **17**(10): 1203-1220.

Lambertsen KL, Gramsbergen JB, Sivasaravanaparan M, Ditzel N, Sevelsted-Moller LM, Olivan-Viguera A, Rabjerg M, Wulff H and Kohler R (2012) Genetic KCa3.1-Deficiency Produces Locomotor Hyperactivity and Alterations in Cerebral Monoamine Levels. *PLoS One* **7**(10): e47744.

Lamoral-Theys D, Pottier L, Kerff F, Dufrasne F, Proutiere F, Wauthoz N, Neven P, Ingrassia L, Antwerpen PV, Lefranc F, Gelbcke M, Pirotte B, Kraus JL, Neve J, Kornienko A, Kiss R and Dubois J (2010) Simple di- and trivanillates exhibit cytostatic properties toward cancer cells resistant to pro-apoptotic stimuli. *Bioorg Med Chem* **18**(11): 3823-3833.

Li N, Timofeyev V, Tuteja D, Xu D, Lu L, Zhang Q, Zhang Z, Singapuri A, Albert TR, Rajagopal AV, Bond CT, Periasamy M, Adelman J and Chiamvimonvat N (2009) Ablation of a Ca2+-activated K+ channel (SK2 channel) results in action potential prolongation in atrial myocytes and atrial fibrillation. *J Physiol* **587**(Pt 5): 1087-1100.

Lipinski CA, Lombardo F, Dominy BW and Feeney PJ (2001) Experimental and computational approaches to estimate solubility and permeability in drug discovery and development settings. *Adv Drug Deliv Rev* **46**(1-3): 3-26.

Meseguer V, Karashima Y, Talavera K, D'Hoedt D, Donovan-Rodriguez T, Viana F, Nilius B and Voets T (2008) Transient receptor potential channels in sensory neurons are targets of the antimycotic agent clotrimazole. *J Neurosci* **28**(3): 576-586.

Milkau M, Kohler R and de Wit C (2010) Crucial importance of the endothelial K+ channel SK3 and connexin40 in arteriolar dilations during skeletal muscle contraction. *FASEB J* **24**(9): 3572-3579.

Mishra RC, Belke D, Wulff H and Braun AP (2013) SKA-31, a novel activator of SK(Ca) and IK(Ca) channels, increases coronary flow in male and female rat hearts. *Cardiovasc Res* **97**(2): 339-348.

Olivan-Viguera A, Valero MS, Murillo MD, Wulff H, Garcia-Otin AL, Arbones-Mainar JM and Kohler R (2013) Novel phenolic inhibitors of small/intermediate-conductance Ca(2)(+)-activated K(+) channels, KCa3.1 and KCa2.3. *PLoS One* **8**(3): e58614.

Radtke J, Schmidt K, Wulff H, Kohler R and de Wit C (2013) Activation of KCa 3.1 by SKA-31 induces arteriolar dilatation and lowers blood pressure in normo- and hypertensive connexin40-deficient mice. *Br J Pharmacol* **170**(2): 293-303.

Rosa JC, Galanakis D, Ganellin CR, Dunn PM and Jenkinson DH (1998) Bis-quinolinium cyclophanes: 6,10-diaza-3(1,3),8(1,4)-dibenzena-1,5(1,4)-diquinolinacyclodecaphane (UCL 1684), the first nanomolar, non-peptidic blocker of the apamin-sensitive Ca^{2+}-activated K^+ channel. *J Med Chem* **41**(1): 2-5.

Ruggieri P, Mangino G, Fioretti B, Catacuzzeno L, Puca R, Ponti D, Miscusi M, Franciolini F, Ragona G and Calogero A (2012) The inhibition of KCa3.1 channels activity reduces cell motility in glioblastoma derived cancer stem cells. *PLoS One* **7**(10): e47825.

Sankaranarayanan A, Raman G, Busch C, Schultz T, Zimin PI, Hoyer J, Kohler R and Wulff H (2009) Naphtho[1,2-d]thiazol-2-ylamine (SKA-31), a new activator of KCa2 and KCa3.1 potassium channels, potentiates the endothelium-derived hyperpolarizing factor response and lowers blood pressure. *Mol Pharmacol* **75**(2): 281-295.

Shakkottai VG, do Carmo Costa M, Dell'Orco JM, Sankaranarayanan A, Wulff H and Paulson HL (2011) Early changes in cerebellar physiology accompany motor dysfunction in the polyglutamine disease spinocerebellar ataxia type 3. *J Neurosci* **31**(36): 13002-13014.

Soder RP, Parajuli SP, Hristov KL, Rovner ES and Petkov GV (2013) SK channel-selective opening by SKA-31 induces hyperpolarization and decreases contractility in human urinary bladder smooth muscle. *Am J Physiol Regul Integr Comp Physiol* **304**(2): R155-163.

Strobaek D, Brown DT, Jenkins DP, Chen YJ, Coleman N, Ando Y, Chiu P, Jorgensen S, Demnitz J, Wulff H and Christophersen P (2013) NS6180, a new K(Ca) 3.1 channel inhibitor prevents T-cell activation and inflammation in a rat model of inflammatory bowel disease. *Br J Pharmacol* **168**(2): 432-444.

Taylor MS, Bonev AD, Gross TP, Eckman DM, Brayden JE, Bond CT, Adelman JP and Nelson MT (2003) Altered expression of small-conductance Ca2+-activated K+ (SK3) channels modulates arterial tone and blood pressure. *Circ Res* **93**(2): 124-131.

Tharp DL, Wamhoff BR, Wulff H, Raman G, Cheong A and Bowles DK (2008) Local delivery of the KCa3.1 blocker, TRAM-34, prevents acute angioplasty-induced coronary smooth muscle phenotypic modulation and limits stenosis. *Arterioscler Thromb Vasc Biol* **28**(6): 1084-1089.

Toyama K, Wulff H, Chandy KG, Azam P, Raman G, Saito T, Fujiwara Y, Mattson DL, Das S, Melvin JE, Pratt PF, Hatoum OA, Gutterman DD, Harder DR and Miura H (2008) The intermediate-conductance calcium-activated potassium channel KCa3.1 contributes to atherogenesis in mice and humans. *J Clin Invest* **118**(9): 3025-3037.

Tuteja D, Xu D, Timofeyev V, Lu L, Sharma D, Zhang Z, Xu Y, Nie L, Vazquez AE, Young JN, Glatter KA and Chiamvimonvat N (2005) Differential expression of small-conductance Ca2+-activated K+ channels SK1, SK2, and SK3 in mouse atrial and ventricular myocytes. *Am J Physiol Heart Circ Physiol* **289**(6): H2714-2723.

Valero MS, Pereboom D, Barcelo-Batllory S, Brines L, Garay RP and Alda JO (2011) Protein kinase A signalling is involved in the relaxant responses to the selective beta-oestrogen receptor agonist diarylpropionitrile in rat aortic smooth muscle in vitro. *J Pharm Pharmacol* **63**(2): 222-229.

Van Der Velden J, Sum G, Barker D, Koumoundouros E, Barcham G, Wulff H, Castle N, Bradding P and Snibson K (2013) K(Ca)3.1 channel-blockade attenuates airway pathophysiology in a sheep model of chronic asthma. *PLoS One* **8**(6): e66886.

Vandorpe DH, Shmukler BE, Jiang L, Lim B, Maylie J, Adelman JP, de Franceschi L, Cappellini MD, Brugnara C and Alper SL (1998) cDNA cloning and functional characterization of the mouse Ca2+-gated K+ channel, mIK1. Roles in regulatory volume decrease and erythroid differentiation. *J Biol Chem* **273**(34): 21542-21553.

Wei AD, Gutman GA, Aldrich R, Chandy KG, Grissmer S and Wulff H (2005) International Union of Pharmacology. LII. Nomenclature and molecular relationships of calcium-activated potassium channels. *Pharmacol Rev* **57**(4): 463-472.

Werkman TR, Kawamura T, Yokoyama S, Higashida H and Rogawski MA (1992) Charybdotoxin, dendrotoxin and mast cell degranulating peptide block the voltage-activated K+ current of fibroblast cells stably transfected with NGK1 (Kv1.2) K+ channel complementary DNA. *Neuroscience* **50**(4): 935-946.

Wulff H and Castle NA (2010) Therapeutic potential of KCa3.1 blockers: recent advances and promising trends. *Expert Rev Clin Pharmacol* **3**(3): 385-396.

Wulff H, Gutman GA, Cahalan MD and Chandy KG (2001) Delineation of the clotrimazole/TRAM-34 binding site on the intermediate conductance calcium-activated potassium channel, IKCa1. *J Biol Chem* **276**(34): 32040-32045.

Wulff H and Kohler R (2013) Endothelial small-conductance and intermediate-conductance KCa channels: an update on their pharmacology and usefulness as cardiovascular targets. *J Cardiovasc Pharmacol* **61**(2): 102-112.

Wulff H, Kolski-Andreaco A, Sankaranarayanan A, Sabatier JM and Shakkottai V (2007) Modulators of small- and intermediate-conductance calcium-

activated potassium channels and their therapeutic indications. *Curr Med Chem* **14**(13): 1437-1457.

Wulff H, Miller MJ, Hansel W, Grissmer S, Cahalan MD and Chandy KG (2000) Design of a potent and selective inhibitor of the intermediate-conductance Ca^{2+}-activated K^+ channel, IKCa1: a potential immunosuppressant. *Proc Natl Acad Sci U S A* **97**(14): 8151-8156.

Zhang M, Pascal JM, Schumann M, Armen RS and Zhang JF (2012) Identification of the functional binding pocket for compounds targeting small-conductance Ca(2)(+)-activated potassium channels. *Nat Commun* **3**: 1021.

Zhang Q, Timofeyev V, Lu L, Li N, Singapuri A, Long MK, Bond CT, Adelman JP and Chiamvimonvat N (2008) Functional roles of a Ca2+-activated K+ channel in atrioventricular nodes. *Circ Res* **102**(4): 465-471.

A

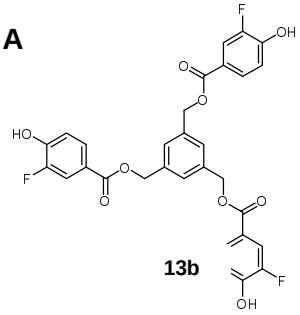

MW: 582 D
LogP: 6.0

13b

B

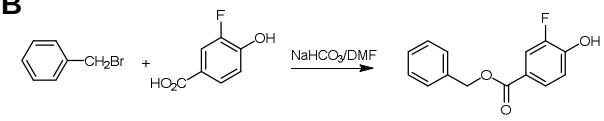

RA-1 MW: 246 D; LogP: 3.4

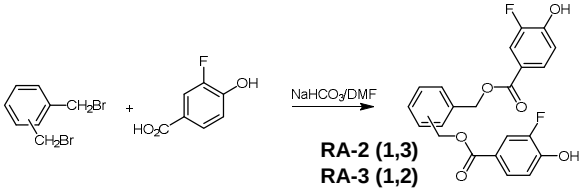

RA-2 (1,3)
RA-3 (1,2)
RA-4 (1,4)

MWs: 414 D
LogPs: 4.7

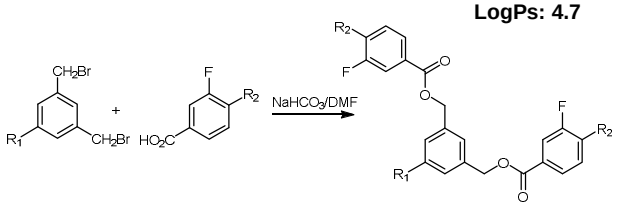

RA-5: R_1=H, R_2=NHAc **MW: 496 D; LogP: 3.3**
RA-6: R_1=CH_2OH, R_2=OH **MW: 444 D; LogP: 4.1**

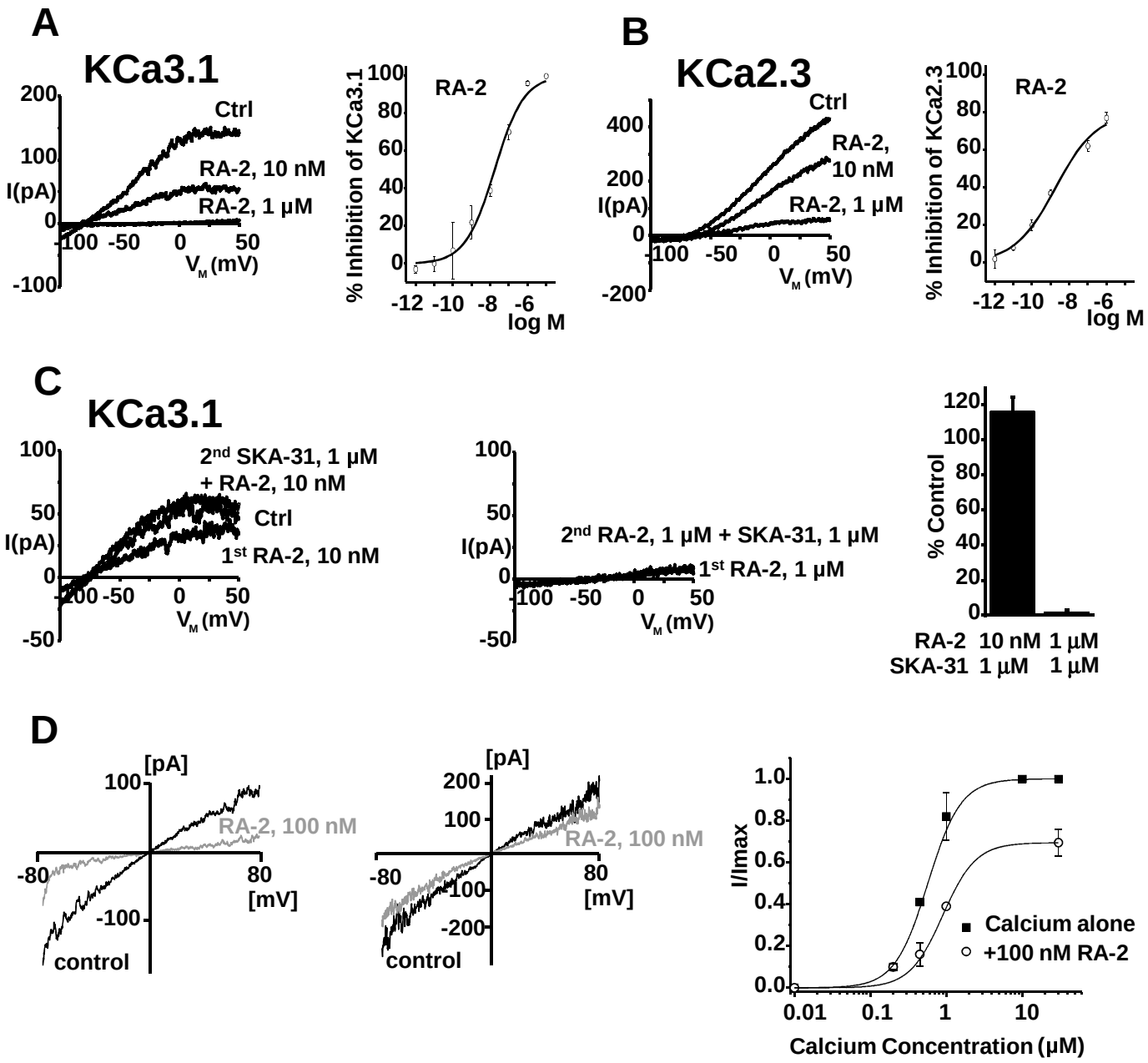
A
KCa3.1
Ctrl
RA-2, 10 nM
RA-2, 1 µM
I(pA)
V_M (mV)
% Inhibition of KCa3.1
RA-2
log M
B
KCa2.3
Ctrl
RA-2, 10 nM
RA-2, 1 µM
I(pA)
V_M (mV)
% Inhibition of KCa2.3
RA-2
log M
C
KCa3.1
2nd SKA-31, 1 µM + RA-2, 10 nM
Ctrl
1st RA-2, 10 nM
I(pA)
V_M (mV)
2nd RA-2, 1 µM + SKA-31, 1 µM
1st RA-2, 1 µM
% Control
RA-2 10 nM 1 µM
SKA-31 1 µM 1 µM
D
[pA]
RA-2, 100 nM
control
[mV]
I/Imax
Calcium alone
+100 nM RA-2
Calcium Concentration (µM)

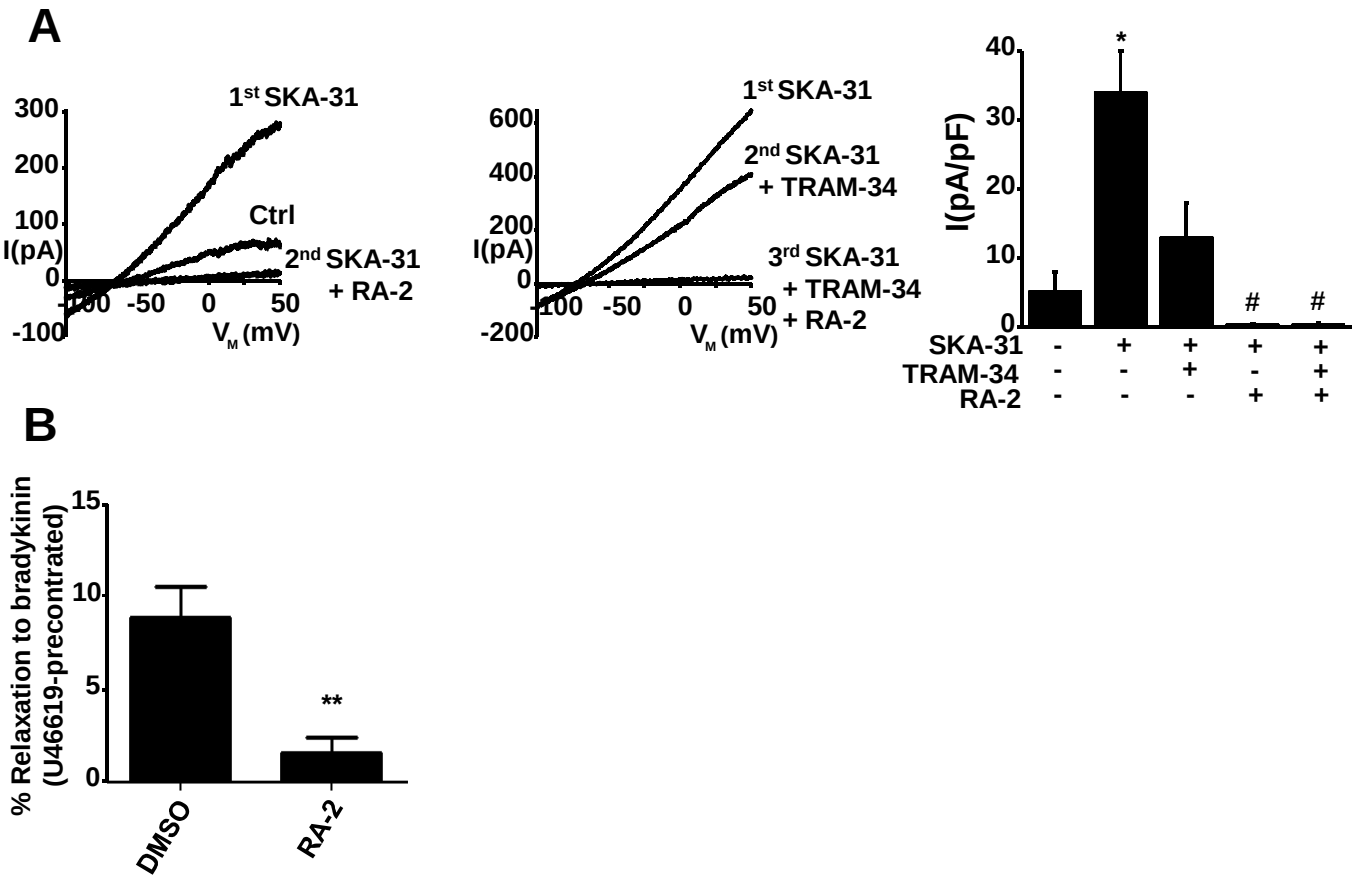
A
1st SKA-31
Ctrl
2nd SKA-31
+ RA-2
I(pA)
VM (mV)
1st SKA-31
2nd SKA-31
+ TRAM-34
3rd SKA-31
+ TRAM-34
+ RA-2
I(pA/pF)
SKA-31
TRAM-34
RA-2
B
% Relaxation to bradykinin
(U46619-precontrated)
DMSO
RA-2

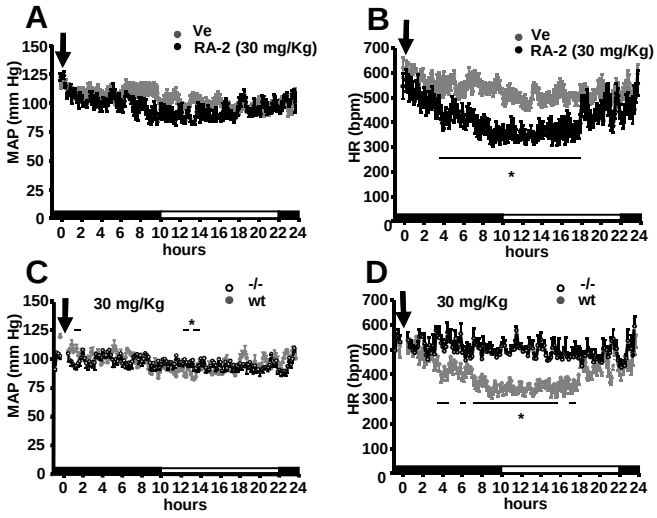
A
Ve
RA-2 (30 mg/Kg)
MAP (mm Hg)
150
125
100
75
50
25
0
0 2 4 6 8 10 12 14 16 18 20 22 24
hours
B
Ve
RA-2 (30 mg/Kg)
HR (bpm)
700
600
500
400
300
200
100
0
*
0 2 4 6 8 10 12 14 16 18 20 22 24
hours
C
30 mg/Kg
-/-
wt
MAP (mm Hg)
*
0 2 4 6 8 10 12 14 16 18 20 22 24
hours
D
30 mg/Kg
-/-
wt
HR (bpm)
*
0 2 4 6 8 10 12 14 16 18 20 22 24
hours

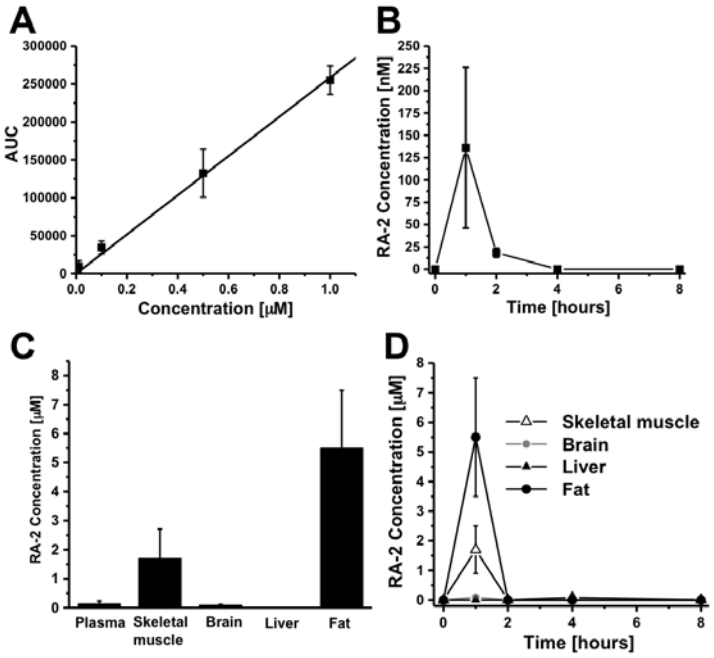
A
AUC
Concentration [μM]
B
RA-2 Concentration [nM]
Time [hours]
C
RA-2 Concentration [μM]
Plasma
Skeletal muscle
Brain
Liver
Fat
D
RA-2 Concentration [μM]
Skeletal muscle
Brain
Liver
Fat
Time [hours]

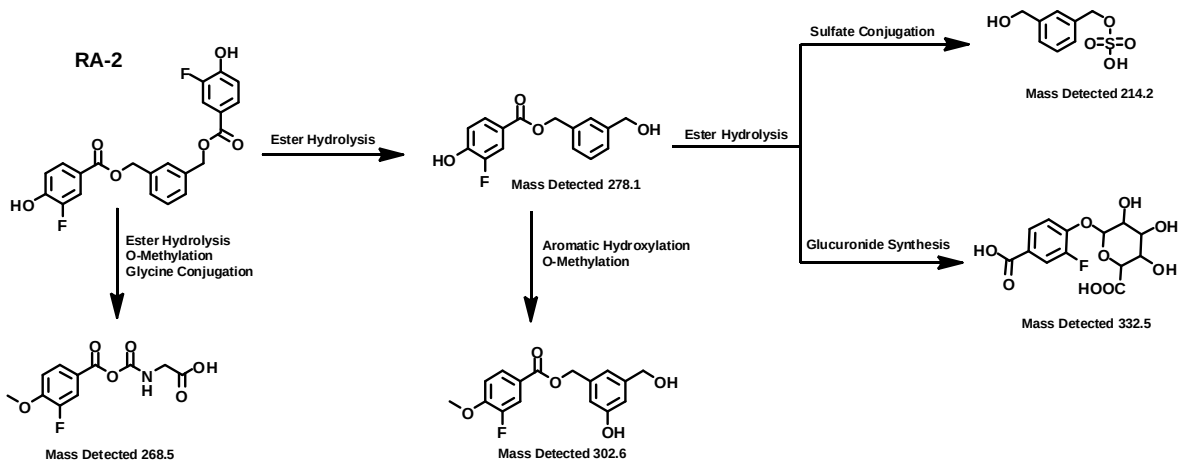
RA-2
Ester Hydrolysis
Ester Hydrolysis
O-Methylation
Glycine Conjugation
Mass Detected 268.5
Mass Detected 278.1
Aromatic Hydroxylation
O-Methylation
Mass Detected 302.6
Ester Hydrolysis
Sulfate Conjugation
Mass Detected 214.2
Glucuronide Synthesis
Mass Detected 332.5